Korean J. of Chem. Eng., **12**(2), 168-175 (1995)

MATHEMATICAL ANALYSIS AND EXPERIMENTAL RESULTS OF APPLYING ENHANCED-SURFACE-AREA PACKED-BED ELECTRODES IN ELECTROGENERATIVE SULFUR DIOXIDE OXIDATION

Jongwook Lee† and Stanley H. Langer*

Energy Research & Development Team, Samsung Electronics,
416 Maetan-3Dong Paldal-Gu, Suwon City, Kyungki-Do 441-742, Korea
*Department of Chemical Engineering, University of Wisconsin, Madison, WI 53706, U.S.A.
(*Received 14 February 1994 • accepted 13 January 1995*)

Abstract—The results of applying enhanced-surface-area packed-bed (ESAP) electrodes in electrogenerative SO_2/O_2 cells are reported to illustrate their utility and potential applications. Mathematical analysis with parameters pertinent to the experimental conditions shows that all electrocatalyst sites in these electrodes are expected to be uniformly utilized for electrochemical SO_2 oxidation. Experimental results showed that ESAP electrodes (1 mg Pt/cm^2) could provide at least 5 times higher SO_2 conversion at given cell voltages than graphite sheet electrodes (1.5 mg Pt/cm^2).

Key words: *Electrogenerative, Sulfur Dioxide, Packed Bed, Electrode*

INTRODUCTION

The electrochemical oxidation of sulfur dioxide (SO_2) has been of special interest because it can be involved in a number of electrochemical processes associated with the treatment of effluent waste gases, and possibly related to some energy conversion cycles [Hollax et al., 1968; Langer and Sakellaropoulos, 1979; Lu and Ammon, 1980; Scott and Winnick, 1988; Struck et al., 1982; Townley and Winnick, 1981; Winnick, 1990]. In earlier work involving the development of liquid-phase electrogenerative SO_2/O_2 cells [Card et al., 1988; Lyke and Langer, 1991a], graphite sheet-supported platinum anodes were initially used because of their high conductivity, inertness, and macroporosity for electrolyte flow, all important requirements for packed-bed operation. However, the relatively small surface area (5-20 m^2/g) of the commercially available support has limited catalyst dispersion in the packed-bed. To enhance the packed-bed electrode performance, an increase in effective surface area of the packed-bed electrodes was needed. At the same time, it was undesirable to have a pressure-drop increase for electrolyte flow through the packed-bed from any additional surface area (e.g., activated carbon bed (200-1000 m^2/g) [Card et al., 1990a]). While there have been other investigations into more efficient packed-bed electrodes for obtaining higher current densities [Fleet, 1990; Oloman, 1983], these increases were often associated with surface area increase and/or facilitation of the mass-transport processes.

The approach adapted here for increasing the effective surface area of packed-bed electrodes for electrochemical SO_2 processing was to fabricate them by utilizing platinum electrocatalyst supported on high-surface-area, carbon black microporous structures and attaching them to relatively large graphite particles so that a bulk macroporous structure for the bed was maintained (see Fig. 1a)

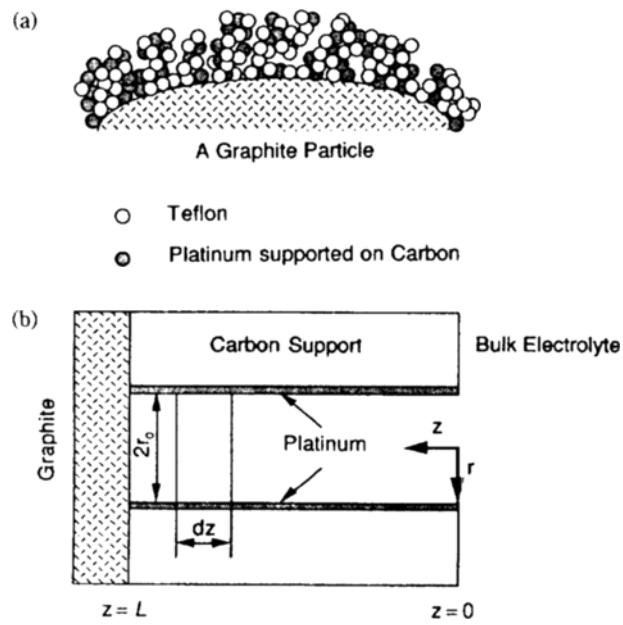

Fig. 1. Models for an enhanced-surface-area electrocatalyst. (a) Physical representation, (b) Mathematical model.

[McIntyre and Phillips, 1982; McIntyre and Phillips, 1984]. This general approach with operation in the electrogenerative mode makes it possible to adapt the large-surface-area carbon blacks so widely used in gas diffusion electrode fabrication [Kinoshita, 1988] to packed-bed electrode application. Thus it could realize some of the promise of flow through porous electrode operation [Newman and Tiedemann, 1975]. Heretofore, the large pressure drop for microporous beds and high contact resistance between small particles have limited the use of such electrocatalysts. The attachment of the finer carbon black-supported platinum electrocatalyst to larger graphite particles allows macroporosity to be compatible with enhanced active surface. The contact resistance

†To whom all correspondences should be addressed.
Present Address: Battery R&D Team, Samsung Display Devices, 575 Shin-Ri Taean-Eub Hwasung-Kun, Kyungki-do 445-970, Korea

Table 1. Parameters in this work

Dimension of the packed-bed = 5.08 cm × 1.27 cm, 0.3175 cm thick
Diameter of particles in the packed-bed, $d_P = 0.149$ cm
Bed voidage of the packed-bed, $\varepsilon = 0.477$
Superficial velocity of anolyte in the packed-bed, $v = 3.69$ cm/sec
Conductivity of 3 M H_2SO_4, $\kappa = 0.27\ \Omega^{-1}\ cm^{-1}$
Kinematic viscosity of 3 M H_2SO_4, $\nu = 1.5 \times 10^{-2}$ cm²/sec
Density of 3 M H_2SO_4, $\rho = 1.2$ g/cm³
Diffusivity of SO_2 in 44 wt% H_2SO_4, $D = 10^{-5}$ cm²/sec
Exchange current density of SO_2 oxidation, $i_o = 10^{-11}$ A/cm²
Reynold number, $Re = vd_P/\nu = 37$
Schmidt number, $Sc = \nu/D = 1500$

of the packed-beds also tends to decrease in comparison with activated carbon (or carbon black) packed-beds. Because of the larger bulk graphite particle networks, commercially available active catalytic materials of different types can also be incorporated into the structure.

Here, the results of applying these enhanced-surface-area packed-bed (ESAP) electrodes for electrogenerative SO_2 oxidation are reported to illustrate their utility and potential applications. Mathematical analysis with parameters pertinent to this work allows consideration of electrocatalyst utilization as well as limitations of ESAP types of electrode advantages.

MATHEMATICAL ANALYSIS

1. External Mass Transfer Limiting Currents

Mass-transfer processes for the enhanced-surface-area (ESA) particles (see Fig. 1a) can be considered in terms of two general processes: external mass transfer between the bulk electrolyte and the external surfaces of these particles, and internal mass transfer between the external surfaces of these particles and the small particle electrocatalyst surfaces in the finer internal pore surfaces. The former must be considered prior to the latter because the former can determine the maximum rate of the latter.

An external mass transfer rate for the packed-bed electrode can be estimated with the mass transfer coefficient which can be calculated by the Wilson and Geankoplis correlation [Wilson and Geankoplis, 1966]:

$$\frac{\varepsilon\, d_P\, k_m}{D} = 1.09\left(\frac{v\, d_P}{D}\right)^{1/3} \tag{1}$$

where ε is the void fraction of packed-bed; d_P is the particle diameter; k_m is the mass transfer coefficient; D is the diffusivity; v is the superficial-velocity of a flowing-through electrolyte. This correlation is valid when the Reynold number is between 0.0016 and 50 and Schmidt number is between 950 and 70600. To calculate the mass transfer coefficient with Eq. (1), the packed-bed electrode is assumed to be composed of spherical particles with diameter, d_P. The Reynold number and the Schmidt number of the packed-bed electrode in this case are calculated as shown in Table 1.

With the parameters in Table 1, the mass transfer coefficient is calculated as 0.0058 cm/sec. Now the mass transfer limiting current can be calculated as nFk_msLC, where n is the number of electrons involved in an electrochemical reaction; F is the Faraday constant; s is the specific surface area of the packed-bed electrode; L is the thickness of the packed-bed electrode; C is the reactant concentration. If the particles are regarded as spheres which have no internal pores, the minimum external surface area of the packed-bed can be calculated. With the particle diameter shown at Table 1, it is approximately 21 cm^{-1}. Therefore the minimum external mass transfer limiting current density in the packed-bed electrode can be calculated as 7500 mA/cm² when the SO_2 concentration is 0.9 M. In practice, currents up to 185 mA/cm² have been observed with the ESAP electrode in this study. This means that the external mass transfer between the bulk electrolyte and the external surfaces of the particles is insignificant in the overall mass transfer process. In the following, the electrocatalyst utilization in the small pores of the ESAP electrode is investigated with a mathematical model.

2. Electrocatalyst Utilization in Small Pores

The electrocatalyst utilization in the small pores of enhanced-surface-area particles would essentially depend on the interaction of local electrode kinetics at electrocatalyst surfaces along the pore walls with the transport of reactants and products to/from electrocatalyst surfaces. While the total electrocatalytic active area can be increased significantly with the large-surface-area carbon black support, electrocatalyst particles in the small pores may not be utilized uniformly due to pore diffusional limitations. One consequence can be a nonuniform distribution of reactants and currents. To understand this problem, a mathematical model based upon transport processes and local reaction kinetics is considered. The electrocatalyst utilization in the small pores of ESAP particles can be treated with an approach resembling the simple pore-model treatment of gas-diffusion electrodes [Austin et al., 1965; Srinivasan, 1967; Srinivasan et al., 1967; Srinivasan and Hurwitz, 1967].

The model for the enhanced-surface-area particle then is an array of cylindrical micropores closed at one end (see Fig. 1b) with electrocatalytic materials essentially located at the pore wall. Electrocatalysts on the outside and at the pore bottom are neglected because of its small area relative to that deposited on the pore walls. The potential along the pore wall is treated as uniform. With radial diffusion neglected, the situation is simplified to one where a one-dimensional model can be used. This can be justified on the basis of the activation-controlled current density being less than the radial-diffusion-limited current density [Austin et al., 1965], which implies that

$$i_o \exp\left[\frac{(1-\alpha)nF\eta}{RT}\right] < \left(\frac{DnFC^b}{r_o}\right) \tag{2}$$

where i_o is the exchange current density; α is the charge transfer coefficient; n is the number of electrons involved in the electrochemical reaction; F is the Faraday constant; η is the overpotential; R is the gas constant; T is the temperature; D is the diffusivity; C^b is the bulk concentration, and r_o is the pore radius. The left side is the resulting current density from the Butler-Volmer Equation for anodic reaction without mass-transfer limitations; the right side represents the limiting current density for radial diffusion in the pore [Srinivasan and Hurwitz, 1967]. Using the typical experimental conditions ($\alpha = 0.5$; $\eta = 0.3$ V; $T = 298$°K; $C^b = 1.0 \times 10^{-3}$ mol/cm³; r_o (measured) $= 1.0 \times 10^{-6}$ cm), the left side of Eq. (2) becomes 1.19×10^{-6} A/cm² in comparison with 1.93×10^{3} A/cm² for the right side. Thus radial diffusion is indeed a negligible factor and the one-dimensional model is justified. In the ranges of our experiments with parameter variation, the activation-controlled current density still tends to be less than the

calculated radial-diffusion-limited current density by 5 orders of magnitude or more.

At steady state, the net flux of reactant into the pore is equal to the total current generated there. For a material balance over the differential element of the pore length of Fig. 1b,

$$\pi r_o^2\left(-D\frac{dC}{dz}\right)_z=\pi r_o^2\left(-D\frac{dC}{dz}\right)_{z+\Delta z}+\frac{d(I_Z)}{nF} \tag{3}$$

With the small pore electrolyte essentially stagnant, convection need not be considered. The local concentration change of the oxidized species from the reaction (SO_4^{2-} in SO_2 oxidation) in this strong sulfuric acid supporting electrolyte is also negligible.

The generated current in an element dz now becomes a function of potential and species concentrations in the electrolyte. Using Butler-Volmer kinetics [Srinivasan, 1967], the current density, i, is

$$i=i_o\left[\frac{C_{ox}}{C_{ox}^b}\exp\left(-\frac{\alpha nF\eta}{RT}\right)-\frac{C_{red}}{C_{red}^b}\exp\left\{\frac{(1-\alpha)nF\eta}{RT}\right\}\right] \tag{4}$$

For high overpotentials in the anodic reaction at the pore wall surface, this becomes

$$d(I_Z)=2\pi r_o dz i_o\left[-\frac{C}{C^b}\exp\left(\frac{(1-\alpha)nF\eta}{RT}\right)\right] \tag{5}$$

where I_Z is the local current generated in the pore from $z=0$ to $z=z$ and C_{red} is designated as C for convenience. With substitution of Eq. (5) into (3),

$$\frac{d^2C}{dz^2}-\frac{m^2}{L^2}C=0 \tag{6}$$

$$\text{where } m^2=\frac{2i_oL^2\exp\left[\frac{(1-\alpha)nF\eta}{RT}\right]}{nFDr_oC^b} \tag{7}$$

Here L is the pore length. Boundary conditions for Eq. (6) then are:

$$C=C^b \quad \text{at } z=0 \tag{8}$$

$$\left(\frac{dC}{dz}\right)=0 \quad \text{at } z=L \tag{9}$$

The boundary condition in Eq. (8) simplifies the concentration profile at the pore inlet. The solution of this type of problem then is:

$$\frac{C}{C^b}=\frac{\cosh[m(1-x)]}{\cosh m} \tag{10}$$

with dimensionless length, $x=z/L$. With the assumption that the total generated current in the pore, I_T, is equivalent to the molar flux at the pore entrance.

$$I_T=-\frac{\pi r_o^2DnF}{L}\left(\frac{dC}{dx}\right)_{x=0} \tag{11}$$

From Eq. (10),

$$\left(\frac{dC}{dx}\right)_{x=0}=-C^b m\tanh m \tag{12}$$

so that

$$I_T=\frac{\pi r_o^2DnFC^b}{L}m\tanh m \tag{13}$$

There are two limiting cases in Eq. (13). When m is very small, tanh m can be approximated as m. Thus Eq. (13) becomes

$$I_T=\frac{\pi r_o^2DnFC^b}{L}m^2 \tag{14}$$

$$=2\pi r_oLi_o\exp\left[\frac{(1-\alpha)nF\eta}{RT}\right] \tag{15}$$

When m is very large, tanh m can be approximated as 1.

$$I_T=\frac{\pi r_o^2DnFC^b}{L}m \tag{16}$$

$$=(2r_o^3\pi^2DnFC^bi_o)^{1/2}\exp\left[\frac{(1-\alpha)nF\eta}{2RT}\right] \tag{17}$$

Therefore one can observe the Tafel slope as twice of the original slope, and the exchange current density as the square root of the original. This situation occurs when the diffusion rate is much slower than the electrochemical reaction rate.

Now the current from the entrance to any distance, x, in the pore can be calculated using

$$I_Z=-\frac{\pi r_o^2DnF}{L}\left[\left(\frac{dC}{dx}\right)_{x=0}-\left(\frac{dC}{dx}\right)_{x=x}\right] \tag{18}$$

$$=-\frac{\pi r_o^2DnFC^b}{L}\left[-m\tanh m+\frac{m\sinh\{m(1-x)\}}{\cosh m}\right] \tag{19}$$

Therefore we can estimate current distribution (electrocatalyst utilization) in the pore anywhere along the wall, using the following equation [Austin et al., 1965; Srinivasan et al., 1967].

$$\frac{I_Z}{I_T}=\frac{\sinh m-\sinh[m(1-x)]}{\sinh m} \tag{20}$$

Using the SO_2 oxidation exchange current density, 10^{-11} A/cm^2 from Appleby and Pichon [Newman, 1991], severe mass-transfer problems are not expected to occur along the pores of the enhanced-surface-area particles under the conditions of experiments here. All electrocatalyst sites along the pore are expected to be uniformly utilized for SO_2 oxidation.

EXPERIMENTAL

1. Preparation of ESAP Electrodes

ESAP electrodes were prepared using graphite particles (Superior Graphite Company, 9012 Desulco, US Mesh 16-18). The preparation of ESAP electrodes involves two major steps : (i) deposition of platinum on the Vulcan XC-72R (Cabot Corporation, surface area: 254 m^2/g, particle size: 30 nm), and (ii) attachment of the Vulcan XC-72R-supported platinum catalyst to the larger graphite particles [McIntyre and Phillips, 1982].

To increase wettability through surface oxidation [Kinoshita, 1988; Goodenough et al., 1990; Drazic and Adzic, 1969] and conductivity through partial graphitization [Kinoshita, 1988], the Vulcan XC-72R support was treated first in flowing carbon dioxide at 950℃ for 1 hour in a tube furnace. Following this treatment, platinum was deposited on the Vulcan XC-72R by the reduction of aqueous chloroplatinic acid using hydrazine [Goodenough et al., 1990; Kinoshita and Stonehart, 1977]. Aqueous hexachloroplatinic acid solution (Johnson Matthey, Inc.) containing 10 wt% platinum based on the Vulcan XC-72R weight was neutralized to pH 7 with sodium bicarbonate (Mallinckrodt, Inc.) and then added to the suspension. The suspension was heated at 80℃ for 2 hours

Table 2. Surface area of platinum electrocatalysts

Sample[a]	Pt loading (mg Pt/cm²)	BET surface (m²/g)	Pt surface[b] (m²/g Pt)	Pt dispersion (%)
Pt/graphite sheet	1.5	0.39	15.7	7
Pt/ESA particle[d]	1.0	9.25	118.0	44

[a]Cross sectional geometric area of the packed-bed is 6.45 cm².
[b]Platinum area is estimated from an electrochemical technique, assuming 210 μC/cm² Pt.
[c]Weight used for packed-bed electrode is 2.47 g.
[d]Weight used for packed-bed electrode is 1.30 g.

with continuous stirring to allow colloidal platinum particle deposition on the Vulcan XC-72R. In order to reduce adsorbed platinum salt on the Vulcan XC-72R, 50-fold excess hydrazine (Aldrich Chemical Company, Inc.) was added to the suspension and the dispersion was then heated at 80℃ for 1 hour with continous stirring to complete the reduction process. The Vulcan XC-72R electrocatalyst was then washed with deionized water, and the suspension filtered using a 1.0 μm Teflon membrane. It was then dried at room temperature overnight followed by 140℃ in air over 1 hour.

The dried Vulcan XC-72R electrocatalyst was dispersed in water under ultrasonication for 10 minutes. A small amount of isopropyl alcohol was added to help wetting. Then a small amount of Cab-O-Sil (Cabot, Grade M-5) was added to the suspension and mixed under ultrasonication for 5 minutes. Cab-O-Sil promoted mechanical integrity of enhanced-surface-area particles. Then 0.01 g of Teflon (du Pont Company, Teflon 30B) was added to the suspension with further mixing. After this, the larger graphite particles (3.00 g) were added to the suspension and the suspension was mixed completely. The mixture was then heated at 220℃ for water removal with stirring to prevent particle agglomeration. When the slurries became dry, they were cooled to room temperature, washed with isopropyl alcohol, and then with water. After drying at room temperature overnight, the particles were placed in an oven at 140℃ for 1 hour.

2. Electrode Characterization

The total surface area and the platinum surface area of the electrodes were measured. The total surface area was obtained using a single-point N_2 BET method in a standard-flow-type surface analyzer (Micromeritics Flowsorb II 2300). The platinum area was obtained in an electrochemical three compartment cell in which working electrode was separated from a platinum wire counter electrode by a glass frit and the NaCl-saturated calomel electrode accessed to the working electrode by a Luggin capillary. The experimental setup and the theory of this technique, where the electrode potential is perturbed as a linear function of time while the current generated by the surface processes is recorded, has been published elsewhere [Kinoshita, 1988; Bard and Faulkner, 1982; Gileadi, 1967]. The results are shown in Table 2.

3. Electrogenerative Cells and Apparatus

The electrogenerative cell was a hybrid-sandwich type incorporating a packed-bed anode with an electrolyte-impermeable, gas-diffusion type cathode separated by both an electrolyte and a membrane (RAI Research, R4010) [Lyke and Langer, 1991a; Card et al., 1990b]. The cell body was constructed from stress-relieved polypropylene and gaskets were prepared from Teflon and Viton. A schematic representation of the assembled electrogenerative cell with auxiliary circuit is shown respectively in Fig. 2.

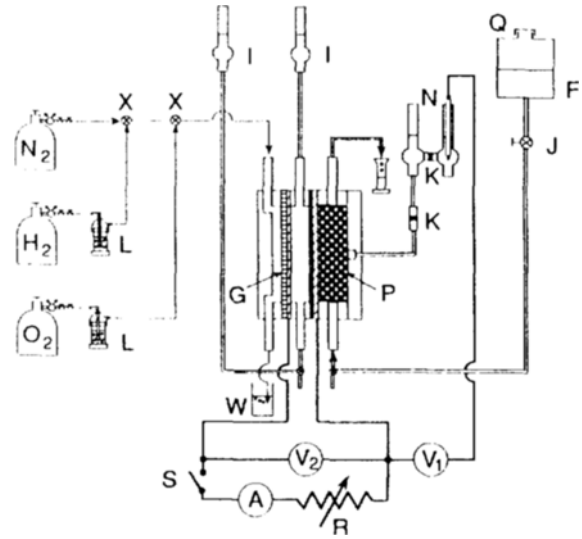

Fig. 2. Schematic representation of the electrogenerative cell and associated circuitry.

(A) Ammeter
(F) Feed
(G) Gas diffusion electrode
(I) Catholyte reservoir
(J) Valve with PTFE plug
(K) Fine glass frit
(L) Gas sparger with water
(N) NaCl-saturated calomel electrode
(P) Packed-bed electrode
(Q) Glass cap
(R) Variable resistor
(S) Switch,
(V_1, V_2) High impedance voltmeters
(W) Beaker with water
(X) Three-way valve

ESAP electrodes were used for SO_2 oxidation in conjunction with a commercial platinum black gas-diffusion-electrode as a cathode [Lyke and Langer, 1991a; Card et al., 1990b]. All of the SO_2 anodes in this work were sulfur-activated by the procedure developed for packed-bed electrodes [Lyke and Langer, 1991a; Seo and Sawyer, 1964; Seo and Sawyer, 1965]. To prepare the packed-bed electrode, enhanced-surface-area particles were placed into the packed-bed chamber and slightly compressed by a platinum screen current collector placed in front of the bed.

4. Cell Polarization Experiments

Electrolyte (3 M H_2SO_4) was prepared with reagent-grade sulfuric acid and then purged with argon for 1 hour or more to remove any dissolved oxygen. Desired SO_2 concentrations in the 3 M H_2SO_4 were obtained by mixing 3 M H_2SO_4 saturated with SO_2 at room temperature and pressure with appropriate amounts of fresh 3 M H_2SO_4. The SO_2 concentrations here were kept below 0.9 M to minimize bubble formation in the packed-bed. Fully saturated 3 M H_2SO_4 at ambient conditions was determined to be 1.16 M SO_2 by an idiometric method [Lyke and Langer, 1991a; Huss et al., 1982], close to the 1.1 M at 20℃ estimated by Card et al. [Card et al., 1988].

After all the cell parts were assembled, ESAP anodes and LAA-2 cathodes were conditioned before cell polarization experiments to assure reproducible results. To reduce platinum oxides on LAA-2 electrodes, hydrogen was fed to the cathode gas compartment. After 10 minutes of hydrogen treatment of the cathode, anode and cathode were connected through a variable resistor, and a current of 10 mA was drawn from the cell through the variable resistor. When the current at short circuit fell below 10 mA, the resistor was replaced with the constant-current supply

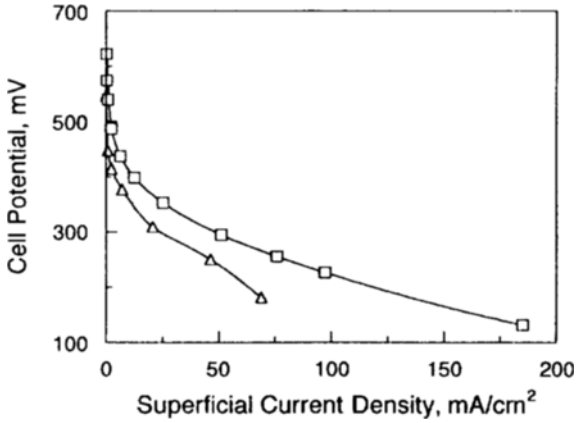

Fig. 3. Performance curves for electrogenerative SO_2/O_2 cells. Anode: (□) ESAP electrode (1.0 mg Pt/cm²), (△) graphite-sheet packed-bed electrode (1.5 mg Pt/cm²); Cathode: LAA-2; Anolyte: 0.9 M SO_2 in 3 M H_2SO_4, 3.7 cm/min; Catholyte: 3 M H_2SO_4, static; Membrane: RAI-4010; 25°C. R_{int} = 0.09 Ω. Polarization curves are corrected for IR losses.

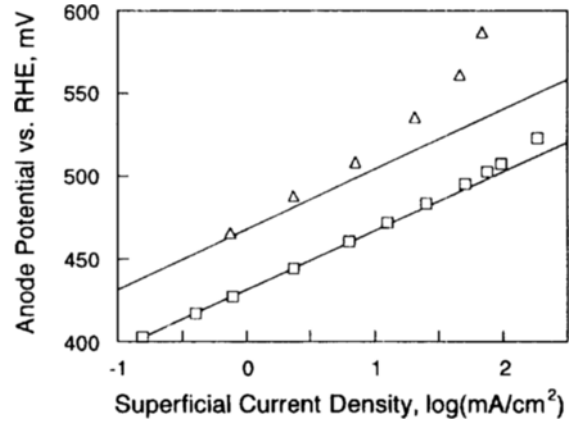

Fig. 4. Polarization of packed-bed anodes under load. (□) ESAP electrode (1.0 mg Pt/cm²); (△) graphite sheet packed-bed electrode (1.5 mg Pt/cm²). (Same conditions as Fig. 3).

in series with the ammeter across the cell. Currents of 10 mA or less were then applied to keep the cell potential at 0.0 to 0.5 mV (slightly cathodic to the packed-bed) with the cathode hydrogen gas feed maintained. Slight hydrogen-gas-bubble production, observed at the ESAP anode during the pretreatment, was removed from the chamber at the anode outlet. After 30 minutes of reduction, with the constant-current supply off, the NaCl-saturated calomel electrode (SSCE) potential vs. the cathode with its adsorbed hydrogen was recorded. This provided a potential referenced to a reversible hydrogen electrode (RHE). Careful electrode pretreatment resulted in minimum internal resistance and reproducible cell polarization behavior.

Polarization curves were obtained by decreasing the external resistor load from open circuit. Each potential in a polarization experiment was determined after three minute equilibration at the reported superficial current density to obtain a steady-state value. The superficial current density is the total current divided by the cross sectional area of electrodes used here (50.8 mm × 12.7 mm). The anode potential was never allowed to exceed 750 mV vs. RHE to limit any irreversible oxide formation which can diminish electrocatalytic activity for SO_2 oxidation [Appleby and Pichon, 1979; Comtat and Mahenc, 1969].

RESULTS AND DISCUSSION

1. The Performance of ESAP Electrodes for SO_2 Oxidation

The performance of the ESAP electrode and the graphite sheet packed-bed electrode [Lu and Spotnitz, 1981] are compared as anodes for SO_2 oxidation in electrogenerative SO_2/O_2 cells in Figs. 3 and 4 for platinum loadings of 1.0 mg Pt/cm² and 1.5 mg Pt/cm² respectively. Three-molar aqueous sulfuric acid electrolyte was used since this fell in the range of the best performance at room temperature [Card et al., 1988; Lyke and Langer, 1991a]. High SO_2 concentrations in the anolyte assured that cell performance was studied under kinetically-limiting conditions with minimal concentration polarization effects. To minimize SO_2 gas bubble complications, however, SO_2 concentrations were limited to a 0.9 M maximum.

As can be seen from Figs. 3 and 4, the performance of ESAP electrode was superior to that of the graphite sheet packed-bed electrode. With ESAP electrodes in SO_2/O_2 cells, a current density of 185 mA/cm² could be achieved. This is equivalent to a calculated SO_2 oxidation rate of 6.19×10^{-6} mol SO_2/s in the 2 cm³ packed-bed (50.8 mm × 12.7 mm × 3.2 mm). The ESAP electrode is about 90 mV less polarized at 70 mA/cm² than the graphite sheet packed-bed electrode, demonstrating the capacity for electrogeneratively oxidizing at a considerably higher cell potential. Much of the cell improvement comes from the enhanced-active-surface area of the ESAP electrode. In Table 2, where surface areas are compared, it can be seen that the ESAP electrode (platinum area: 0.76 m²) has a platinum surface area 5 times higher than the graphite sheet packed-bed electrode (platinum area: 0.15 m²), even though the total ESAP electrode platinum loading (1.0 mg Pt/cm²) is only 2/3 of the loading of the graphite sheet electrode (1.5 mg Pt/cm²). The platinum dispersion in the ESAP electrode (44%) is enhanced through use of the high-surface-area Vulcan XC-72R support. However, use of the Teflon binder for the attachment to the larger graphite particles could limit platinum site use for the carbon-supported platinum catalyst in the finished product. Thus the platinum surface area of the ESAP electrode based on electrochemical measurement is only 74% of the original Vulcan XC-72R catalyst platinum surface area (159 m²/g Pt) before fabrication to the ESAP electrode. This loss can be kept low through use of minimal Teflon (5 wt% based on the Valcan XC-72R weight) in the ESAP fabrication.

A Tafel slope for the SO_2 oxidation on sulfur-activated finely-dispersed platinum particles can also be estimated from the plot in Fig. 4. Since the packed-bed potential was measured relative to SSCE located at the back of the packed-bed, a consideration was given to estimating a Tafel slope with correction for the average packed-bed potentials [Lyke and Langer, 1991b; Newman and Tiedemann, 1978; Newman and Tobias, 1962]. Potentials of the front and the back of the ESAP electrode were measured under the same conditions as those of Fig. 4. The potential difference of the front and the back of the 3.2 mm thick packed-bed was at most 3 mV below 2.3 mA/cm² and reached 66 mV at 81 mA/cm². Since there can be difficulties in estimating the average packed-bed potential at higher current densities, a reasonable Ta-

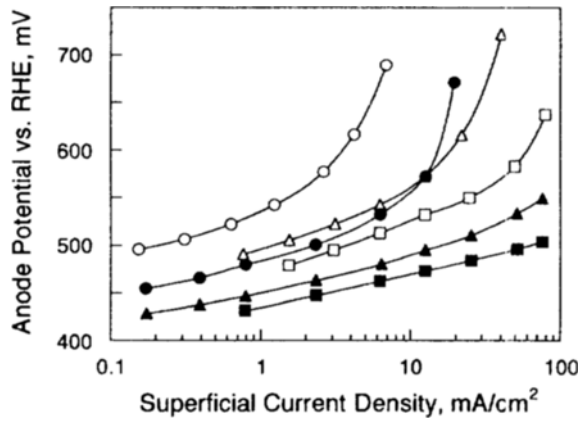

Fig. 5. Tafel plot for graphite-sheet packed-bed electrodes and ESAP electrodes at comparable SO_2 concentrations. Anode: (■, ▲, ●) ESAP electrode (1.0 mg Pt/cm²), (□, △, ○) graphite-sheet packed-bed electrode (1.5 mg Pt/cm²); Cathode: LAA-2; Anolyte: (□, ■) 0.5 M, (△, ▲) 0.1 M, (○, ●) 0.01 M SO_2 in 3 M H_2SO_4; Catholyte: 3 M H_2SO_4, static; Membrane: RAI-4010; 25 to 26°C. (See text).

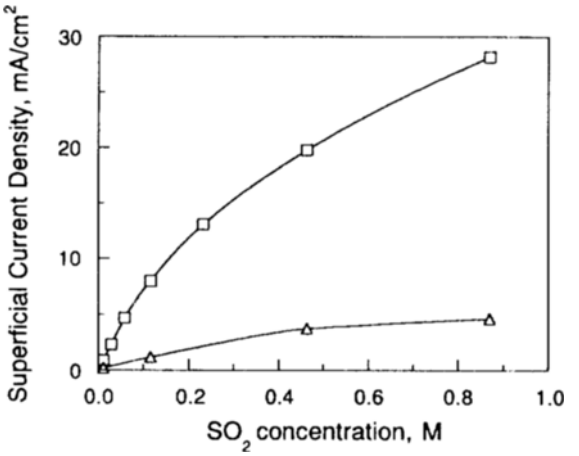

Fig. 6. Comparison of ESAP and graphite-sheet electrode activities at constant anode potential at 500 mV vs. RHE. (□) ESAP electrodes (1.0 mg Pt/cm²), (△) graphite sheet electrodes (1.5 mg Pt/cm²). (Same conditions as Fig. 5).

fel line was constructed by limiting the data to the low-current-density region (below 2.3 mA/cm²) where any error would be less than 3 mV, assuming ESAP electrode pore concentration polarization is insignificant at these low current densities. The calculated Tafel slope is then 36 mV/decade on our sulfur-activated finely-dispersed platinum particles (average size: 15 to 25 Å). This slope can be compared to the values reported in the literature: 44 mV/decade [Katagiri et al., 1973] and 45 mV/decade [Appleby and Pichon, 1979] for smooth bulk platinum electrodes which do not seem to be sulfur-activated [Lyke and Langer, 1991a; Seo and Sawyer, 1965] and 40 mV/decade for graphite sheet-supported platinum particles which were sulfur-treated [Lyke and Langer, 1991a].

2. The Effect of SO_2 Concentrations on Electrogenerative SO_2/O_2 Cells

The performances of ESAP electrodes are compared further with that of the graphite sheet packed-bed electrodes [Lyke and Langer, 1991a] at various SO_2 concentrations in Fig. 5. In fairly concentrated solutions such as 0.5 M, ESAP electrodes polarize significantly less than graphite sheet electrodes at high current densities since the large platinum area reduces polarization. At 0.1 M SO_2, the SO_2/O_2 cell with the ESAP electrodes produced about 80 mA/cm² while the anode potential still stayed below 600 mV vs. RHE. At 0.01 M SO_2, significant polarization appeared in the ESAP electrode, and the maximum current density fell to 20 mA/cm². In contrast, the graphite sheet electrode shows polarization at 0.5 M SO_2 even with increased SO_2 solution feed rates, so that the resulting current density is well below that for the ESAP electrode under the same conditions.

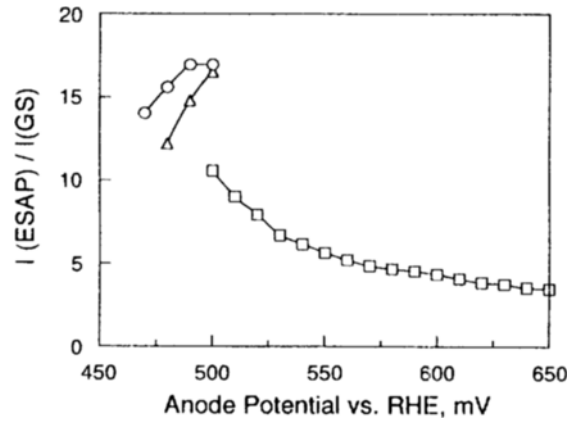

Fig. 7. Ratio of currents produced in ESAP electrodes to those in graphite sheet (GS) electrodes at selected potentials and concentrations. (○) 0.9 M, (△) 0.5 M, (□) 0.01 M SO_2 in 3 M H_2SO_4. (Same conditions as Fig. 5).

The activities of ESAP electrodes and the graphite sheet packed-bed electrodes are compared in a different way at 500 mV vs. RHE in Fig. 6. ESAP electrodes (1.0 mg Pt/cm²) with increased exposed platinum area support a current 5 times higher than that produced with graphite sheet electrodes (1.5 mg Pt/cm²) over the entire range of SO_2 concentrations. The ratios of the currents from the ESAP electrode to those of the graphite sheet electrode also agree well with their platinum area ratio. This result also shows that the platinum activity changes associated with dispersion (or particle size) are minor since the platinum particle sizes in these electrodes are quite different [approximately 20 Å (ESAP) vs. 150 Å (graphite sheet)].

3. The Activities of Packed-Beds

The activities of the ESAP electrodes and graphite sheet packed-bed electrodes of our work are compared further at several electrode potentials of interest and SO_2 concentrations in Fig. 7. Since a desirable mode of electrogenerative cell operation would be with fast reaction rate (high current density) at high cell potential, several ratios of currents produced in the ESAP electrode to those produced in the graphite sheet packed-bed electrode at the same electrode potential are presented. On the basis of the ratios of platinum areas of the ESAP electrode (0.76 m²) and the graphite sheet electrode (0.15 m²), the current density ratio would be about 5 if all platinum sites in both electrodes were utilized efficiently without concentration polarization from diffusional limitations in small pores.

In concentrated SO_2 solutions at the level of 0.5 or 0.9 M, ESAP electrodes produced current densities 12 to 17 times higher than the graphite sheet packed-bed electrodes with the current ratio

Table 3. Electrical conductivity of packed-bed electrodes

Sample	Electrical conductivity ($\Omega^{-1}\cdot cm^{-1}$)	Electrical resistance of a packed bed ($10^2\ \Omega$)	
		without 3 M H_2SO_4	with 3 M H_2SO_4
GSPE (1.5 mg Pt/cm^2)	12.0	2.0	2.0
ESAPE (1.0 mg Pt/cm^2)	7.0	2.3	2.0
Graphite particles (no pt)	9.8	2.1	2.0
Copper plate	-	1.6	-

increasing with rising anode potential. This reflects a situation where the graphite sheet electrode performance even at high SO_2 concentrations is apparently limited because of relatively small exposed platinum area. This conclusion is supported by the more rapid increase of the ratio at 0.5 M than at 0.9 M SO_2. Apparently the reduced platinum particle size of the ESAP structure allows reactants to be transported more effectively by spherical diffusion than by planar diffusion when pore diffusional limitations are not a factor. The finely-dispersed platinum crystallite catalyst then is particularly advantageous.

With the more dilute 0.01 M SO_2 solution, the ESAP electrode can still produce current densities 11 times higher than the graphite sheet packed-bed electrode at 500 mV vs. RHE. But with higher currents and higher polarization, the ratio decreases as can be seen in Fig. 7. This is because at this low SO_2 concentration level, concentration polarization in the small ESAP electrode pores begins to limit catalyst performance. The ESAP electrode still produced a current density about 3.5 times higher than the graphite sheet electrodes at the highest potential of 650 mV as shown in Fig. 7, but some platinum electrocatalyst in the ESAP electrode is utilized less effectively at higher current densities. This effect at low concentrations would seem to be characteristic because despite large macroscopic flow channels in the packed-bed, performance ultimately depends on the micropore structure and catalyst accessibility.

4. The Conductivity of Packed-Beds

Since the matrix conductivity of ESAP electrodes could be lowered from contact resistance in the Vulcan XC-72R catalyst attachment to the graphite particles with Teflon, the conductivities of a graphite sheet electrode and an ESAP electrode were compared in our standard cell configuration. The conductivity of a graphite particle packed-bed without platinum was also measured to evaluate conductivity effects from the incorporation of Vulcan XC-72R with Pt into the ESAP electrode. The contact resistance between the platinum screen and the packed-bed was also obtained. The contact resistance (7.7 mΩ) between the 6.45 cm^2 packed-bed and the platinum screen was indeed found to be significant compared with the packed-bed resistance ($\approx$20 mΩ). This result confirms the earlier suggestion of Oloman et al. [Oloman et al., 1991] that packed-bed/current collector contact resistance is important for packed-bed-electrode cell design.

The results in Table 3 show that the bulk conductivity of the ESAP electrode (7.0 $\Omega^{-1}\cdot cm^{-1}$) is comparable to that of the graphite sheet packed-bed electrode (12.3 $\Omega^{-1}\cdot cm^{-1}$). The measured bulk conductivity of graphite particles alone (9.8 $\Omega^{-1}\cdot cm^{-1}$) shows that there is only a slight drop from the Vulcan XC-72R catalyst-graphite particle attachment process. In addition to bulk ESAP electrode conductivity, the contact resistance in Vulcan XC-72R catalyst attached via Teflon binder might require future consideration since it may become a limiting factor in the performance of small platinum catalyst particles locally, especially for high-current-density operations.

CONCLUSION

The operation of liquid-phase, electrogenerative SO_2/O_2 cells is considerably increased through use of ESAP electrodes. The improved performance was manifested by higher currents and higher cell voltages than was obtained with a graphite sheet packed-bed electrode in earlier work. The enhancement is a consequence of incorporation of large-surface-area carbon supports into the electrode structure. Although the platinum loading for the ESAP electrode (1.0 mg Pt/cm^2) was 2/3 of the platinum loading of the graphite sheet packed-bed electrode (1.5 mg Pt/cm^2), the exposed platinum surface area was 5 times higher than the graphite sheet electrode. This led to a significantly higher SO_2 oxidation rate at low SO_2 concentrations.

The general approach of attaching fine particles to larger ones for packed-bed use seems to be quite feasible. Mathematical analysis with parameters pertinent to the experimental conditions shows that all electrocatalyst sites in these electrodes are expected to be uniformly utilized for electrochemical SO_2 oxidation. The utilization of a highly dispersed platinum on carbon black (44% dispersion) without a pressure drop increase in the packed-bed compartment was a significant advantage for the ESAP electrode for SO_2 oxidation relative to the earlier graphite sheet electrode (7% dispersion). Advantages of ESAP electrodes in electrogenerative SO_2/O_2 cells include; (i) higher current densities with less electrode polarization, (ii) facilitation of operation at lower substrate concentrations, (iii) a cost saving for platinum catalyst because of improved dispersion on the peripheral high-area support.

ACKNOWLEDGEMENT

This work is supported by the National Science Foundation and the University of Wisconsin-Madison.

REFERENCES

Appleby, A. J. and Pichon, B., "The Mechanism of the Electrochemical Oxidation of Sulfur Dioxide in Sulfuric Acid Solutions", *J. Electroanal. Chem.*, **95**, 59 (1979).

Austin, L. G., Mariet, M., Walker, R. D., Wood, G. B. and Comyn, R. H., "Simple-Pore and Thin-Film Models of Porous Gas Diffusion Electrodes", *Ind. Eng. Chem.*, **4**, 321 (1965).

Bard, A. J. and Faulkner, L. R., "Electrochemical Methods-Fundamentals and Applications", Wiley, New York, 1982.

Card, J. C., Foral, M. J. and Langer, S. H., "Electrogenerative Oxidation of Dissolved Sulfur Dioxide with Packed-Bed Anodes", *Environ. Sci. & Tech.*, **22**, 1499 (1988).

Card, J. C., Valentin, G. and Storck, A., "The Activated Carbon Electrode: A New Experimentally Verified Mathematical Model for the Potential Distribution", *J. Electrochem. Soc.*, **137**, 2736 (1990a).

Card, J. C., Lyke, S. E. and Langer, S. H., "Electrogenerative Oxidation of Model Alcohols at Packed-Bed Anodes", *J. Appl. Electrochem.*, **20**, 269 (1990b).

Comtat, M. and Mahenc, J., "Electrochemical Oxidation of Sulfur Dioxide on a Platinum Electrodes", *Bulletin de la Societe Chimique de France*, **11**, 3862 (1969).

Drazic, D. M. and Adzic, R. R., "Investigation of Active Carbon for Fuel-Cell Electrodes", *Electrochim. Acta*, **14**, 405 (1969).

Fleet, B., "Electrochemistry, Past and Present", Stock, J. T. and Orna, M. V., eds., ACS Symp. Ser., 390, Canada, 1990.

Gileadi, E., "Electrosorption", Plenum press, New York, 1967.

Goodenough, J. B., Hamnett, A., Kennedy, B. J., Manoharan, R. and Weeks, S. A., "Porous Carbon Anodes for the Direct Methanol Fuel Cell-I. The Role of the Reduction Method for Carbon Supported Platinum Anodes", *Electrochim. Acta*, **35**(1), 199 (1990).

Hollax, E., Schwabe, K. and Wiesener, K., "Electrochemical Disposal of Industrial Waste Gases and Development of a Double-Layer Electrodes", DECHEMA Monogr., **59**(1045-1069), 147 (1968).

Huss, A., Jr, Lim, P. K. and Eckert, C. A., "Oxidation of Aqueous Sulfur Dioxide. 1. Homogeneous Manganese(II) and Iron(II) Catalysis at Low pH", *J. Phys. Chem.*, **86**, 4224 (1982).

Katagiri, A., Takehara, Z. and Yoshizawa, S., "Oxidation of Sulfur Dioxide on Platinum in Sulfuric Acid", *Denki Kagaku*, **41**, 692 (1973).

Kinoshita, K. and Stonehart, P., "Modern Aspects of Electrochemistry", Vol. 12, Bockris, J. O'M. and Conway, B. E., eds., Chap. 4, Plenum Press, New York, 1977.

Kinoshita, K., "Carbon", John-Wiley & Sons, New York, 1988.

Langer, S. H. and Sakellaropoulos, G. P., "Electrogenerative and Voltametric Processes", *Ind. Eng. Chem. Process Des. Dev.*, **18**(4), 567 (1979).

Lu, P. W. T. and Ammon, R. L., "An Investigation of Electrode Material for the Anodic Oxidation Sulfur Dioxide in Concentrated Sulfuric Acid", *J. Electrochem. Soc.*, **127**(12), 2610 (1980).

Lu, P. W. T. and Spotnitz, R., "An Investigation of Electrode Materials for the Anodic Oxidation of Sulfur Dioxide in Concentrated Sulfuric Acid", *J. Electrochem. Soc.*, **128**(6), 1298 (1981).

Lyke, S. E. and Langer, S. H., "Oxidation of Sulfur Dioxide in Sulfur-Modified Platinum-Graphite Packed-Bed Electrodes", *J. Electrochem. Soc.*, **138**, 1682 (1991a).

Lyke, S. E. and Langer, S. H., "Internal Ohmic Drop Limits on Effectiveness of Packed Bed Electrodes Obeying Tafel Kinetics", *J. Electrochem. Soc.*, **138**, 2327 (1991b).

McIntyre, J. A. and Phillips, R. F., "Electrochemical Process and Plant Design", Alkire, R. C., Beck, T. R. and Varjian, R. D., eds., pp. 79-97, The Electrochemical Society Softbound Proceedings Series, Princeton, NJ, 1982.

McIntyre, J. A. and Phillips, R. F., US patent, **4**, 457953, 1984.

Newman, J. S. and Tobias, C. W., "Theoretical Analysis of Current Distribution in Porous Electrodes", *J. Electrochem. Soc.*, **109**(12), 1183 (1962).

Newman, J. and Tiedemann, W., "Porous Electrode Theory with Battery Applications", *AIChE J.*, **21**(1), 25 (1975).

Newman, J. S. and Tiedemann, W., "Advances in Electrochemistry and Electrochemical Engineering", Delahay, P., ed., Vol. 11, pp. 353-438, Interscience, New York (1978).

Newman, J. S., "Electrochemical Systems", 2nd ed., Prentice-Hall, Inc., Englewood Cliffs, New Jersey, 1991.

Oloman, C., "Tutorial Lectures in Electrochemical Engineering and Technology", Alkire, R. and Chin, D.-T., eds., AIChE Symp. Ser., 79(229), New York, 1983.

Oloman, C., Matte, M. and Lum, C., "Electronic Conductivity of Graphite Fiber Fixed-Bed Electrodes", *J. Electrochem. Soc.*, **138**, 2330 (1991).

Scott, K. and Winnick, J., "Electrochemical Membrane Cell Design for Sulfur Dioxide Separation from Flue Gases", *Gas Sep. & Purif.*, **2**, 23 (1988).

Seo, E. T. and Sawyer, D. T., "Determination of Sulfur Dioxide in Solution by Anodic Voltammetry and U.V. Spectrophotometry", *J. Electroanal. Chem.*, **7**, 184 (1964).

Seo, E. T. and Sawyer, D. T., "Electrochemical Oxidation of Dissolved Sulfur Dioxide at Platinum and Gold Electrodes", *Electrochim. Acta*, **10**, 239 (1965).

Srinivasan, S., "Electrocatalysis", Advances in Catalysis and Related Subjects, Eley, D. D., ed., Vol. 17, Academic Press, New York, 1967.

Srinivasan, S., Hurwitz, H. D. and Bockris, J. O'M., "Fundamental Equations of Electrochemical Kinetics at Porous Gas-Diffusion Electrodes", *J. Chem. Phys.*, **46**(8), 3108 (1967).

Srinivasan, S. and Hurwitz, H. D., "Theory of a Thin Film Model of Porous Gas-Diffusion Electrodes", *Electrochim. Acta*, **12**, 495 (1967).

Struck, B. D., Junginger, R., Neumeister, H. and Dujka, B., "A Three-Compartment Electrolytic Cell for Anodic Oxidation of Sulfur Dioxide and Cathodic Production of Hydrogen", *Int. J. Hydrogen Energy*, 7(1), 43 (1982).

Townley, D. and Winnick, J., "Flue Gas Desulfurization Using an Electrochemical Sulfur Oxide Concentrator", *Ind. Eng. Chem. Process. Des. Dev.*, **20**, 435 (1981).

Wilson, E. J. and Geankoplis, C. J., "Liquid Mass Transfer at very Low Reynolds Numbers in Packed-Beds", *Ind. Eng. Chem. Fund.*, **5**, 9 (1966).

Winnick, J., "Electrochemical Separation of Gases", Advances in Electrochemical Science and Engineering, Gerischer, H. and Tobias, C. W., eds., Vol. 1, p. 205, 1990.